Viscous Effects in the Inception of Cavitation on Axisymmetric Bodies

V. H. ARAKERI

A. J. ACOSTA

Division of Engineering and
Applied Science, California
Institute of Technology,
Pasadena, Calif.

Cavitation inception and development on two axisymmetric bodies was studied with the aid of a Schlieren flow visualization method developed for that purpose. Both bodies were found to exhibit a laminar boundary layer separation; cavitation inception was observed to occur within this region of separated flow. The incipient cavitation index was found to be closely correlated with the magnitude of the pressure coefficient at the location of flow separation on one of the bodies. There is also experimental evidence that events at the site of turbulent reattachment of the separated flow may also greatly influence cavitation inception.

Introduction

ONE of the central problems in cavitation research has been the prediction of the onset or inception of cavitation and the determination of the laws that scale this phenomenon from model studies conducted in the laboratory to prototype conditions. Although much effort has been expended in addressing this problem (see recent reviews [1, 2])[1] it still remains far from being solved. A recent study [3] organized by the International Towing Tank Conference (I.T.T.C.) illustrates some recurring features in this type of cavitation research; it was shown that the incipient cavitation index[2] obtained in different water tunnel facilities throughout the world on one type of geometrically similar axi-symmetric body could differ by a factor of two. Although each of the results in these various facilities may be said to represent "cavitation" it is clear that different phenomena must be observed to account for the wide differences found. To cite an example, tunnel facilities without

---

[1]Numbers in brackets designate References at end of paper.

[2]See Nomenclature. The value of σ at which inception of cavitation occurs is normally known as incipient cavitation index designated by σ_i. When an established cavity is m ade to disappear, one speaks of the point of "desinent" cavitation and the corresponding index as the desinent cavitation index,σ_d.

Nomenclature

D = diameter of the test body

P_t = free stream tunnel static pressure

P_v = vapor pressure of water at its bulk temperature

S = streamwise position along the body surface from the stagnation point

U = free stream tunnel velocity

U_s = velocity at the position of laminar boundary layer separation

X = axial distance from the stagnation point

ν = coefficient of kinematic viscosity

ρ_L = density of water

θ = boundary layer momentum thickness

θ_s = boundary layer momentum thickness at the position of laminar separation

C_p = pressure coefficient given by,
$$\frac{P - P_t}{1/2\rho_L U^2}$$

C_{Pmin} = minimum pressure coefficient

C_{Ps} = pressure coefficient at the position of laminar separation

C_{Ptr} = pressure coefficient at the position of transition in the laminar boundary layer

L_r = length of the laminar separated region as indicated by Schlieren photographs

Re_D = Reynolds number given by, UD/ν

$Re^*_{\theta_s}$ = Reynolds number given by, $U_s\theta_s/\nu$

Re_{Dcrit} = critical Reynolds number at which transition takes place at the position of laminar boundary layer separation

σ = cavitation number based on vapor pressure given by,
$$\frac{P_t - P_v}{1/2\rho_L U^2}$$

$\bar{\sigma_i}$ = average incipient cavitation index

the presence of a "resorber" as a design feature tend to have abundant supply of macroscopic air bubbles in the water approaching the test body. These bubbles "explode" to vaporous cavities as they pass through the low pressure regions of the flow field; on the other hand tunnel facilities which have a resorber tend to have very few macroscopic free air bubbles in the flow and inception under these circumstances is very close to the surface of the test body and in some cases appears in the form of an attached surface cavity [4]. It is apparent that "nuclei" necessary to initiate the phase change that results in the cavitation observed at inception may come from two sources; namely, from within the free stream, or from the surface of the test body itself, nuclei of the first type being termed "stream" nuclei and the latter, "surface" nuclei. Thus cavitation inception may be assumed to be dependent on two main factors, namely, (a) the source or sources of the nuclei, and (b) their potential of growth into macroscopic cavitation. The growth phase is greatly dependent on the pressure history of the nucleus within the flow. Vapor growth is possible only when the local pressure is lower than the vapor pressure of the liquid. However, in certain cases cavitation has been observed to take place for pressures higher than vapor pressure and this has been ascribed by Holl [2] to the growth of the nucleus by gaseous diffusion who terms the first type of cavitation "vaporous" cavitation and the second "gaseous" cavitation. It is important to distinguish between the two for they are subject to quite different scaling laws.

Of the two sources of cavitating nuclei mentioned before, the behavior of macroscopic free stream nuclei outside the boundary layer was first treated by Johnson and Hsieh [5] who pointed out the "screening" effect of the body pressure field in removing nuclei of certain sizes from regions of low pressure. This effect leads to a calculated velocity dependence of the cavitation inception index not unlike that observed. These ideas were further extended with the experiments by Schiebe [6] and Peterson [7] which tend to confirm the existence of the screening effect in flow situations dominated by free stream bubbles. The present work is concerned with flows in which an abundant supply of such free stream nuclei is not present and in which the surface nuclei may be expected to play a more important role. This situation was first studied in detail by Parkin and Kermeen [8] who observed that cavitation inception bubbles on a hemisphere-cylinder body originate within the boundary layer of the body thus influencing significantly the history of the bubbles. Furthermore, they emphasized the role gaseous diffusion could play in the cavitation inception process within the boundary layer region. These original observations do not appear to have been pursued further experimentally although a number of theoretical models based on them have been proposed. However, these have not been successful [2] in satisfactorily explaining the scale effects observed in cavitation inception.

It may be well to mention here that there are several possible viscous flow regimes on a streamlined body which may be of importance in the inception process; these include, (a) laminar boundary layer flow without separation or turbulent transition, (b) laminar boundary layer flow with transition but without any separation, (c) same as (b) but with a turbulent separation after transition, and (d) a laminar boundary layer separation with the subsequent transition in the separated free shear layer. It is to be expected that cavitation inception if it takes place adjacent to the body would be dependent on the flow regime mentioned in the foregoing. At the very least, residence times and the size of the nuclei would be affected, both, items of importance in the concepts of Parkin and later used by Van der Walle [9] and Holl and Kornhauser [10] in their scaling theories. In addition, the transient pressures in the fully developed region of turbulent flow are known to influence the cavitation inception process [11]. Also from this observation, the transition region itself, a location of intense disturbances, might be expected to play a significant role in the inception process. In any case it may be reasoned
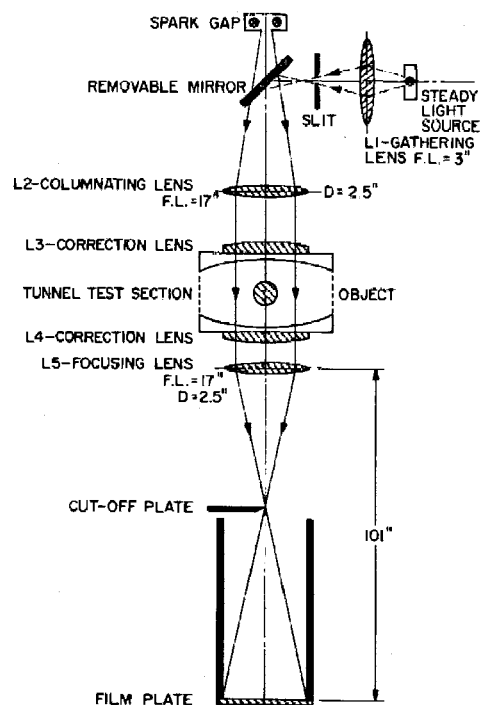
Fig. 1 A schematic diagram of the Schlieren set-up in the high speed water tunnel

that it is misleading or unjustified to draw comparisons about cavitation inception, theory or experiment, without such detailed knowledge. The present work is concerned in particular with determining experimentally the type of viscous flow regime on some of the bodies used in cavitation research, and in what manner cavitation inception may be influenced by the features of these real fluid flows.

Our interest in this approach was prompted by some preliminary boundary layer growth calculations made for the I.T.T.C. test body. These showed that the observed position of cavitation inception roughly coincided with the predicted position of laminar separation which was considerably downstream of the minimum pressure point. It was also found that the value of the inception cavitation number was very close to the pressure coefficient at the predicted position of viscous separation.[3] These findings stimulated us to take another look at the mechanism of cavitation inception on streamlined bodies following the lines of Parkin's original work but augmented with the Schlieren technique borrowed from aeronautics.

Experimental Methods

Conventional methods of flow visualization such as dye injection and oil film techniques are difficult to use in water, especially at high velocities. Preliminary dye injection studies showed the existence of a laminar separation on a two-in. hemispherical half body at a tunnel velocity of about 5 fps. But at a velocity of about 15 fps the observations were difficult to interpret and at speeds higher than this there seemed to be no chance of success. For these reasons we turned to the well-known schlieren technique. The density gradients necessary to the method were created by heating or cooling of the test body. A schematic diagram of the optical setup in the High Speed Water Tunnel (HSWT) is shown in Fig. 1. A similar setup was utilized
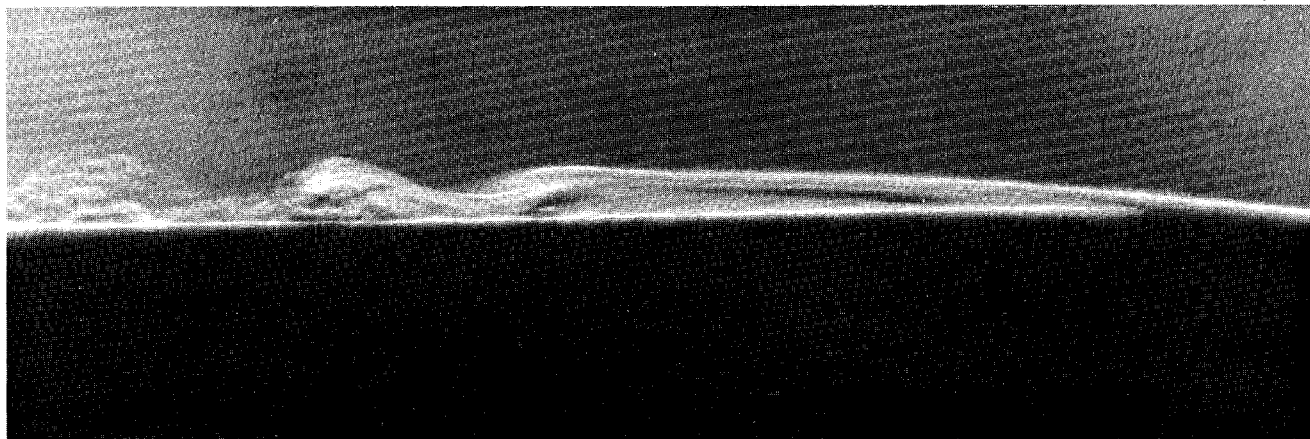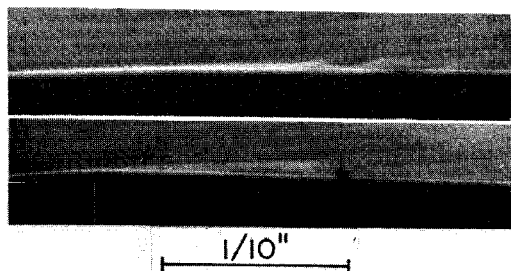

Fig. 2 Laminar separation on a two-in. hemispherical nosed body at a Reynolds number of 10⁵. Also noticed are some details of the reattachment process of the free shear layer. The flow is from right to left and true measure of the maximum height of the separated region is 0.06 in.

for preliminary studies conducted in the Free Surface Water Tunnel (FSWT). A steady light source was used for focusing the optical system and for visual flow observations. A spark source having a duration of approximately 5 to 10μ sec was utilized for still photography. Further details of the apparatus may be found in reference [13], but perhaps it should be noted here that a temperature difference of only 3 to 4 deg F is sufficient to produce a clear thermal boundary layer. Both heating and cooling were shown to produce equivalent effects. In the work to be discussed, heating was used, the source of the heat being a one kw heater immersed within the test bodies. It should be mentioned that the schlieren technique has been used in water by Bland and Pelick [14] but apparently they did not subsequently pursue it further.

Two axisymmetric bodies widely utilized in cavitation inception studies and commonly known as hemispherical nose and "Swedish" Headform[4] (or I.T.T.C. standard headform) were used in the present investigations. The diameter of the hemispherical nose was 1.813 in. and that of the Swedish headform was 1.755 in. The test bodies were mounted in the axisymmetric test section of the HSWT with a three bladed sting support. The bodies occupied less than two percent of the through flow area.

Free stream velocity in the tunnel and cavitation number were determined from tunnel static pressure measurements made with mercury manometers. These computations included corrections for the boundary layer growth along the tunnel walls as outlined in Appendix A of reference [4]. From computations of Hoyt [15] blockage effects are negligible in the present experiments and were not accounted for in the data reduction. The air

---

[4]The Swedish headform is a modified ellipsoidal body of revolution consisting of a tangent ellipse one-half diameter in length and having a flat face with a diameter of one-half the body diameter.

|← 1/10" →|

Fig. 3 Typical photographs showing laminar separation at moderately high Reynolds numbers. Top photograph is of the Swedish headform at Reynolds number of 5.85 x 10⁵ and the bottom is of the hemispherical nosed body at a Reynolds number of 6.04 x 10⁵. Flow is from left to right.

content value of the tunnel water was held fixed at a value of 10 ppm during all test runs and temperature of the water was nominally room temperature. With this value of air content none or very few visible macroscopic air bubbles were seen in the water approaching the test body under all conditions.

Determination of the incipient cavitation condition was made by visual observation under the illumination by a stroboscopic light. In the terminology of Parkin and Kermeen [8] present incipient conditions may be termed "boundary layer incipient cavitation." No attempts were made to record the point of desinent cavitation. Photographs of the boundary layer itself (or more properly the thermal boundary layer) were taken with the schlieren apparatus at a magnification of about 5 times. A "calibration" photograph was made to establish true lengths.

Fully Wetted Flow Observations

Boundary Layer Separation. The effectiveness of the schlieren method of flow visualization technique is clearly illustrated in the photograph of Fig. 2 which shows the laminar boundary layer separation and reattachment of the free shear layer on a two-in. hemispherical nose mounted in the FSWT at a Reynolds number, Re_D, of 10⁵. From such observations it was found that both of the test models possessed a laminar separation "bubble" at all the test velocities used in the HSWT (up to 60 fps). The highest test velocity corresponds to a Re_D of 9.06×10^5 for the hemispherical nose and 8.78×10^5 for the Swedish headform. Examples of laminar separation at a tunnel velocity of 40 fps for both models are shown in the photographs of Fig. 3. From photographs of this type the position of laminar separation was measured and an estimate of the length of the separated region was made. The streamwise position of laminar separation on the hemispherical nose (in both tunnels) and the Swedish headform as a function of tunnel velocity is shown in Fig. 4. From this figure, it may be noted that the position of laminar separation does not change appreciably with tunnel velocity and is not altered by heating or cooling. This assured us that within the present range of temperatures used to create the schlieren effect the boundary layer characteristics were not affected.

In the photographs of Fig. 3, the white line which indicates the boundary of the separated region becomes wavy and subsequently too faint to be recorded. This is evidently the location of intense mixing signaling transition to turbulence; presumably reattachment of the flow would soon follow. In any case it seems reasonable that the representative length of the separated "bubble" is given by this distance. Variation of the distance so measured with velocity for both the test bodies is shown in Fig. 5. As expected the bubble length decreases with increase in velocity for both bodies. Physically these bubble lengths were

quite small, being only 12 percent of the diameter at 20 fps ($\mathrm{Re}_D \doteq 3 \times 10^5$) and about 4 percent at 60 fps ($\mathrm{Re}_D \doteq 9 \times 10^5$).

Comparison With Wind Tunnel Data. The length of separated bubble, L_r, as just defined normalized by the momentum thickness at separation is plotted in Fig. 6 as a function of local Reynolds number. Thwaites' method [26, 27] was used to calculate relevant quantities. Also shown is wind tunnel data obtained by Gaster [16] in his studies on laminar separation bubbles. A measure of length of the separated bubble in his case was found from detail velocity surveys. This "dead air region" scaled as the foregoing agrees well with present findings.

Comparison With Approximate Computations. As mentioned Thwaites' approximate method was used to calculate the boundary layer growth properties. For the hemispherical nose the predicted value of S/D at separation was found to be 0.76 which is actually that observed. The predicted value of S/D at separation for the Swedish headform was found to be 0.82 for all Reynolds numbers whereas, the observed value changes from 0.82 to 0.84 with increase in Re_D of 2.7×10^5 to 8.78×10^5.

It is well known that an attached laminar boundary layer possesses a point of instability at a sufficiently large Reynolds number after which disturbances grow exponentially resulting eventually in transition to turbulence. A semiempirical method developed by Smith, et al. [17] enables one to estimate the approximate position of transition (see Appendix). The Reynolds

Fig. 6 Comparison of present data on length of separated bubble with similar data from wind tunnel studies

number at which transition is to occur at the position of laminar boundary layer separation may be referred to as a "critical Reynolds number" designated by "$\mathrm{Re}_{D\mathrm{crit}}$". Presumably for $\mathrm{Re}_D > \mathrm{Re}_{D\mathrm{crit}}$, no laminar boundary layer separation is possible. Roshko [18] refers to this Reynolds number as "second critical Reynolds number" and finds it to be about 5×10^6 for the case of a cylinder in rectilinear flow. Present computations indicate that $\mathrm{Re}_{D\mathrm{crit}} \doteq 5 \times 10^6$ for the hemispherical nose and that $\mathrm{Re}_{D\mathrm{crit}} \doteq 1.5 \times 10^6$ for the Swedish headform. This is in accord with the present experimental observations that the boundary layer is still laminar at separation at a $\mathrm{Re}_D = 9.06 \times 10^5$ for the hemispherical nose and at a $\mathrm{Re}_D = 8.78 \times 10^5$ for the Swedish headform. During the present experiments it was not possible to attain critical Reynolds number for either of the models. However, it is noteworthy that the length of the separated bubble decreased with increase in Re_D and the length was only 4 percent of the model diameter at Re_D of 8.78×10^5 for the Swedish headform indicating the earlier mentioned estimate of $\mathrm{Re}_{D\mathrm{crit}} \doteq 1.5 \times 10^6$ may be very good.

Normally pressure distribution measurements do indicate the existence of a laminar separation as a constant pressure region. Based on such an observation Rouse [19] states that $\mathrm{Re}_{D\mathrm{crit}} \doteq 2 \times 10^5$ for the hemispherical nosed body whereas from present experiments $\mathrm{Re}_{D\mathrm{crit}}$ is found to be greater than 9×10^5. The erroneous value of $\mathrm{Re}_{D\mathrm{crit}}$ stated by Rouse has resulted from the use of pressure taps with a spacing of 12.5 percent of the body diameter. Thus the resolution of this method is limited to detecting separation bubbles whose lengths are greater than the spacing of the pressure orifices. From present measurements of Fig. 5, it may be noted that for $\mathrm{Re}_D > 2 \times 10^5$ the length of the separated bubble is smaller than 12.5 percent of the body diameter and hence would not be able to be detected by Rouse.

Inception Studies on the Hemispherical Nose

Inception Observations. With the help of the schlieren method it was possible to observe the inception process and the real fluid flow past the body simultaneously. Typical observations afforded by this technique can be seen in Fig. 7. These photographs are spark schlieren pictures on the hemispherical body at three different levels of tunnel pressure and at a tunnel velocity of 40 fps. The dark patches show the form and extent of the incipient and then developing macroscopic cavitation. From Fig. 7(a), the first visible macroscopic cavitation is seen to take place in the reattachment region of the separated flow. It is important to note that inception does not take place in the neighborhood of the minimum pressure point which is expected to lie upstream of the position of laminar separation. The incipient conditions noted in Fig. 7(a) are termed "incipient bubble cavitation" following Kermeen's [20] description of desinent cavitation. As illustrated in Fig. 7(b) reduction in cavitation number produces
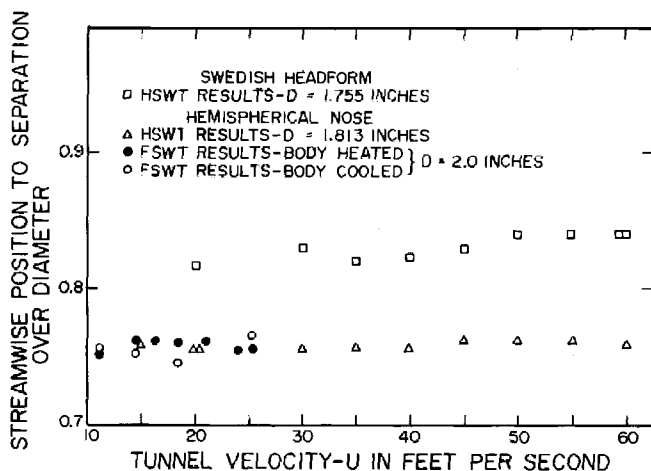

Fig. 4 Measured streamwise position to laminar separation versus tunnel velocity for the Swedish headform and two different hemispherical nosed bodies. Also shown is the effect of heating or cooling on the position of separation.
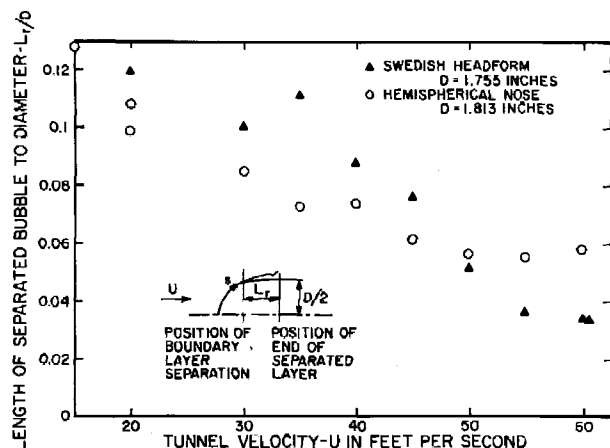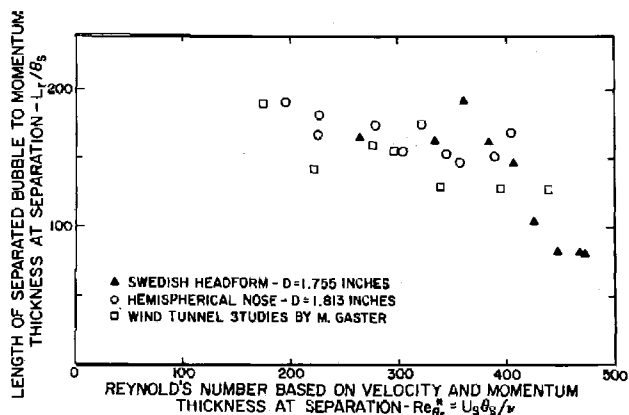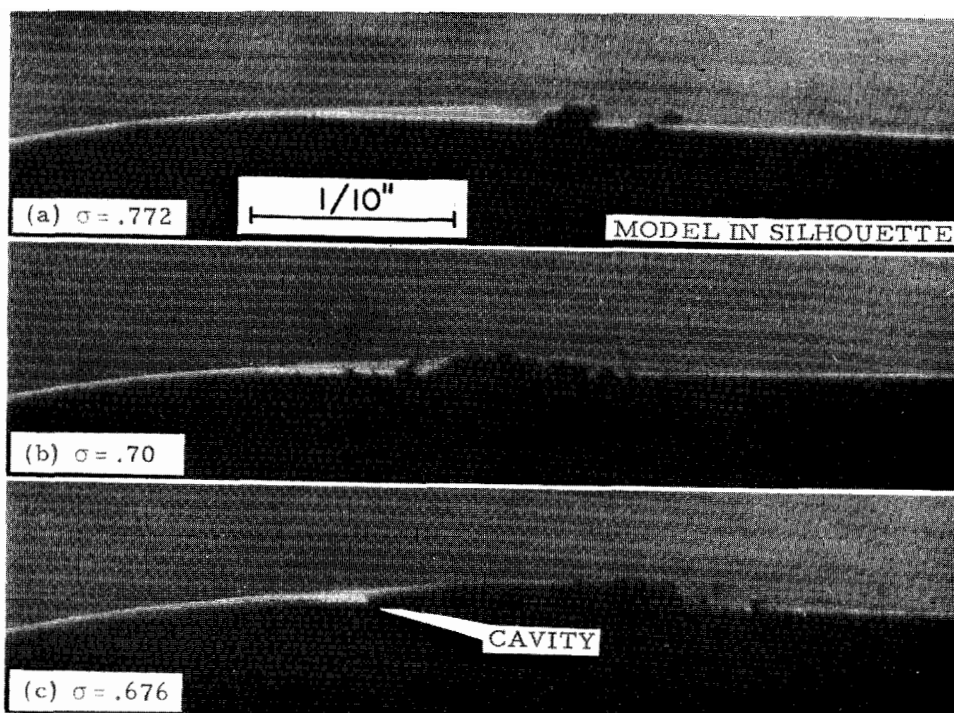

Fig. 5 Length of laminar separated bubble versus tunnel velocity for both the test bodies

Fig. 7 Form and extent of cavitation originating within the viscous separated region of the hemispherical nose at three different levels of tunnel pressure. $U = 40$ fps, Re = 6.04 x 10^5. (The dark patches above the model outline are the cavitating areas.) The flow is from left to right.

increasing amounts of macroscopic cavitation within the separated region; also evident but difficult to observe are very small "microscopic" bubbles which can be seen right up to the point of laminar separation. A further reduction in cavitation number results in the formation of a single macroscopic attached cavity as shown in Fig. 7(c) which exhibits the suppression of the bubble cavitation observed in earlier photographs. The development of cavitation just described was observed to take place for all the test velocities used between 25 to 60 fps, corresponding to Re$_D$ of 3.78×10^5 to 9.06×10^5.

Measurement of bubble sizes in the photographs of Fig. 7(a) and 7(b) showed that the macroscopic bubbles have a diameter approximately equal to the maximum height of the separated region; they were of the order of 0.01 in. in dia and the microscopic bubbles were of the order of 0.0025 in. in dia. These values are in agreement with the previous measurements of Parkin and Kermeen.

Motion pictures taken of cavitation within the separated region with a "Fastax" camera at 4000 frames per sec provided further details of the inception process. In most of the cases observed both macroscopic and microscopic cavitation bubbles originated in the reattachment region of the separated layer. Some of these microscopic bubbles became entrained by the reverse flow of the separated region, and were transported upstream at a velocity of about one fps toward the position of separation. Once reaching the position of separation they traveled downstream within the free shear layer; at present framing rates it was not possible to track these bubbles further. Parkin however observed velocities of a few of these bubbles once in the free shear layer to be between 12 to 26 fps. An example of the observed upstream motion described earlier is provided in the sequential photographs of Fig. 8.

A few bubbles were observed to grow immediately downstream of separation at a fixed position on the body surface as also observed by Parkin and Kermeen; these bubbles were entrained in the free shear layer after growing to diameters equal to that of the local separated height. The important point to note from these complex bubble motions is that residence time within the
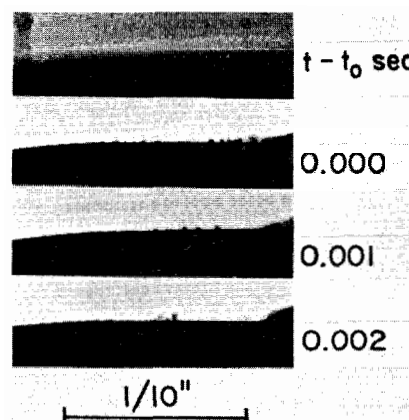
Fig. 8 Typical upstream motion of microscopic cavitation bubbles within the separated region of the hemispherical nose at incipient conditions. Tunnel velocity is 40 ft per sec and the flow is from left to right. At the top is the Schlieren photograph taken at the same velocity and to the same scale.

separated flow region was estimated to be from 1 to 5 millisec and that during this period there was very little growth. Also to be noted is that the growth of the macroscopic bubbles in the reattachment region was quite rapid and could not be photographed in any detail during present studies. Kermeen finds the growth time of these bubbles to be shorter than even a tenth of a millisec.

The present observations of cavitation inception on the hemispherical nose just described strongly suggest that the stationary cavitation bubbles seen on the surface of the body by Parkin [8] were within the viscous separated region of the flow and not submerged in an attached boundary layer as thought. It is easily understood that the stabilization of bubbles was possible since they were within the separated region and did not necessarily require pressure gradient forces for stabilization as thought previously and subsequently considered in detail by Holl and Kornhauser [10] and Van der Walle [9].
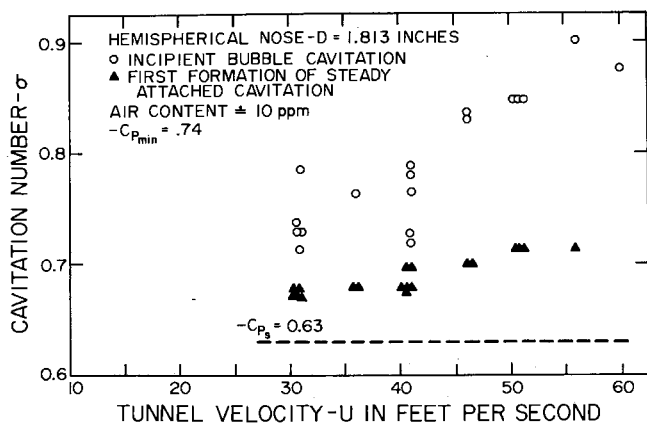
Fig. 9 Cavitation inception data versus tunnel velocity for the hemispherical nose
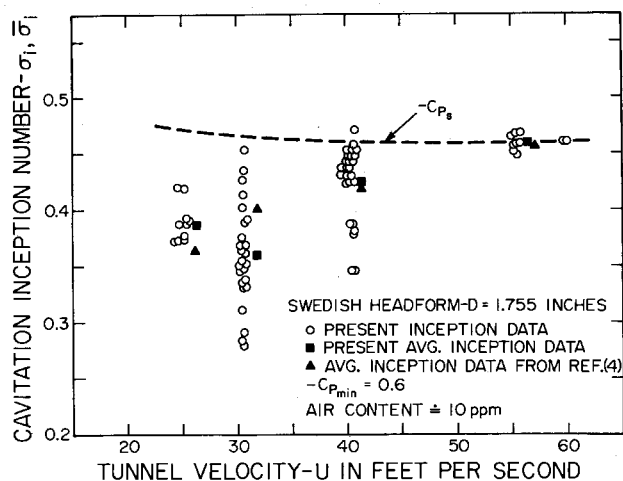

Fig. 10 Cavitation inception data versus tunnel velocity for the Swedish headform. Also shown is the comparison of average inception data with the negative value of the pressure coefficient at the measured position of laminar separation.

transient pressure measurements in these regions preclude further speculation on these interesting points.

As discussed earlier, a reduction in σ below that of σ_i produced more profuse bubble cavitation until eventually a steady, attached macroscopic cavity with a glossy surface was formed. The cavitation index for the occurrence of this type of cavity is shown in Fig. 9 by the filled triangles. It may be noted that these values are also greater than $-C_{p_s}$, indicating that this type of cavitation was sustained by steady gaseous diffusion across the attached cavity walls.

Inception Studies on the Swedish Headform

Observation of Inception. Unlike the hemispherical nose, inception on the Swedish headform was always in the from of a fully developed cavity all around the nose of the headform. This type of inception may be termed "incipient band cavitation" as also done in reference [4]. A typical photograph of inception is shown in Fig. 12 and is marked natural inception. From such photographs, inception was observed to take place in the neighborhood of the position of the boundary layer separa-
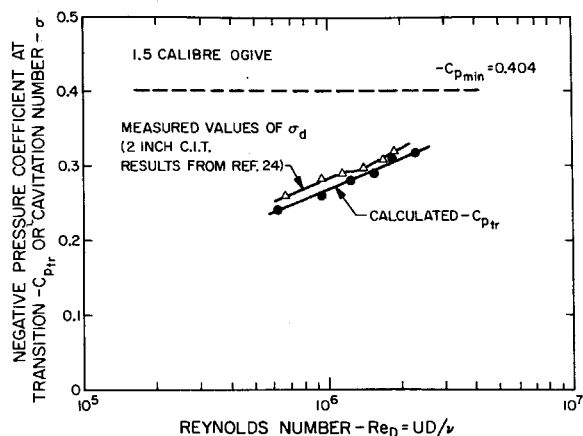

Fig. 11 Comparison of desinent cavitation number for 1.5 caliber ogive with the negative value of the pressure coefficient at the predicted position of transition for $Re_D > Re_{D_{crit}}$

Cavitation Inception Measurements. Fig. 9 shows the incipient cavitation data for the hemispherical nose obtained during present studies. The unfilled circles in Fig. 9 correspond to the incipient conditions termed incipient bubble cavitation. Since inception was seen to occur downstream of the position of laminar separation, naturally the important pressure coefficient to compare σ_i with, would be the negative value of the pressure coefficient at separation, $-C_{p_s}$. The value of $-C_{p_s} = 0.63$ shown in Fig. 9 is obtained with the help of pressure distribution measurements made by Kermeen and the known value of the position of separation in the HSWT shown in Fig. 4. Also shown in Fig. 9 is the value of $-C_{p_{min}} = 0.74$.

It should be noted that σ_i for incipient bubble cavitation at all test velocities is greater than $-C_{p_s}$, indicating that cavitation took place at local static pressures higher than the vapor pressure. This is suggestive that either gaseous cavitation was observed or the strong pressure fluctuations in the reattachment region were responsible for vaporous cavitation. From motion picture studies described earlier one may rule out the possibility of steady gaseous diffusion as the mechanism for the bubble growth, since the residence time of the cavitation bubbles was relatively short and this point has been discussed by Parkin [8] in some detail. It seems possible that a combination of convective gaseous diffusion [21], rectified gaseous diffusion [22] and vaporous cavitation could be responsible for the growth of macroscopic bubbles in the reattachment region; lack of detailed static and
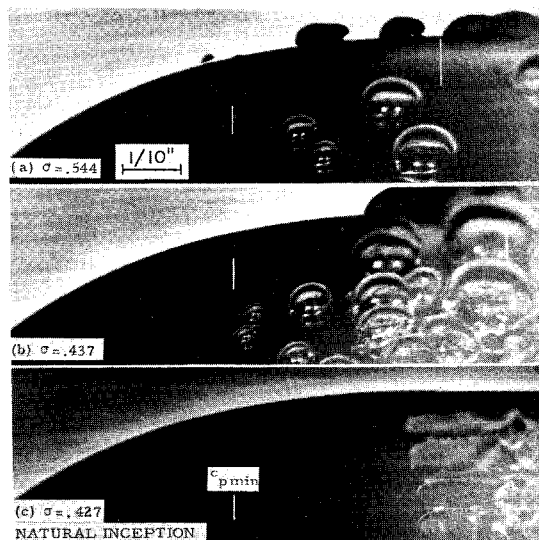

Fig. 12 Photographs illustrating the effect of introducing artificial surface nuclei by electrolysis on the Swedish headform at two different tunnel pressures. Cavitation observed in photographs (a) and (b) would not be present without electrolysis. For comparison photograph (c) shows the natural incipient cavitation. $U = 31$ fps.

tion ($X/D \doteq 0.475$) which existed considerably downstream of the position of minimum pressure point [19] ($X/D \doteq 0.28$). This was the case for all the test velocities which ranged from 25 to 60 fps, corresponding to Re_D of 3.66×10^5 to 8.78×10^5.

Motion pictures taken at 4000 frames per sec of cavitation in the separated region of the Swedish headform produced only sketchy details of the inception process. A large macroscopic cavitation bubble would suddenly appear in the separated region on a frame of the motion picture film and by the next frame a fully developed cavity would be formed. From these observations it was concluded that the inception of cavitation was inherently different on the Swedish headform from that on the hemispherical nose described earlier.

Cavitation Inception Measurements. Fig. 10 shows the incipient cavitation data for the Swedish headform obtained during present studies. Except at a velocity of 30 fps the inception indices reproduce quite well; at 30 fps considerable scatter exists. Comparison of the average incipient index obtained from present data with those obtained earlier by Acosta [4] on the same Swedish headform is shown on the same figure. The average data from both sources are plotted offset to the right by $+0.5$ fps for clarity. The comparison afforded is very good except at a velocity of 30 fps and at this velocity the difference in the $\bar{\sigma}_i$ is about 0.04.

Comparison of $\bar{\sigma}_i$ with $-C_{p_s}$. Also shown in Fig. 10 by dotted line is the negative value of the pressure coefficient at separation which is obtained with the help of pressure distribution measurements made by Rouse [19] and the measured position of the boundary layer separation from Fig. 4. It should be noted that $\bar{\sigma}_i$ is closely related to $-C_{p_s}$ rather than $-C_{pmin}$ which is 0.6 for the Swedish headform. The difference between $\bar{\sigma}_i$ and $-C_{p_s}$ starts with a value of about 0.075 at a velocity of 26 fps and gradually decreases to zero at a velocity of 56 fps.

Some Important Physical Parameters Found in Inception With Separation

We have seen on both test bodies inception of cavitation to be influenced by the presence of laminar separation. However, inception characteristics were different in the sense that $\bar{\sigma}_i > -C_{p_s}$ for the hemispherical nose and $\bar{\sigma}_i < -C_{p_s}$ for the Swedish headform in the same Reynolds number range. Furthermore, the physical appearance of cavitation at inception was different for the two test bodies. From desinent cavitation index measurements by Acosta, one finds that for the Swedish headform not only is the $\bar{\sigma}_i < -C_{p_s}$ but also $\bar{\sigma}_d < -C_{p_s}$. Therefore one may rule out the "hysteresis" [23] effects to be responsible for the aforementioned differences in the inception characteristics for the two test bodies.

One of the principal differences in the nature of real fluid flow past the two bodies was in the observation that height of the separated layer for the case of the hemispherical nose was 2 to 3 times larger than for the case of the Swedish headform. This difference which is apparent from the photographs of Fig. 3 is expected to be at least partially responsible for the different inception characteristics. The difference in height just noted is expected to play an important role in determining the details of transition and reattachment mechanism of the free shear layer (see Gaster [16]) and at least for the hemispherical nose inception was observed to take place in this region. In addition the maximum size of nuclei trapped in the separated region was found to be proportional to the maximum height of the separated region. Under any circumstance, physically important parameters determining the incipient conditions would be: (a) pressure coefficient at the position of laminar separation, C_{p_s}, (b) Reynolds number based on local quantities at separation, $Re^*_{\theta_s}$, and (c) additional length parameter, say H/θ_s where H is the relevant length. It is tempting to think that this length might be proportional to maximum height of the separated region although there is now no basis to determine such a length.

It must be pointed out here that from present experimental work no explanation is found for the observed size effect on σ_i for geometrically similar bodies of a given shape for a fixed Reynolds number. Examples of such dependence are well known and, in particular, Parkin and Holl [24] have observed this effect on a hemispherical body and a 1.5 caliber ogive.

A Cavitation Correlation for Bodies With Attached Boundary Layers

Using the calculation procedure previously mentioned, the position of turbulent transition has been estimated as a function of Re_D for a 1.5 caliber ogive with a cylindrical afterbody. Re_{Dcrit} for this body is estimated to be 6.3×10^5. Knowing the position of transition and pressure distribution on the headform [19], one can determine the value of the pressure coefficient at this point designated by C_{ptr}. A comparison of $-C_{ptr}$ and desinent cavitation number for a two-in. 1.5 caliber ogive taken from reference [24] is shown in Fig. 11. These results show that there is a close correlation of σ_d with $-C_{ptr}$.

The foregoing finding is yet to be verified by direct observation of transition. However, in the case of separated flows, inception occurred in the reattachment region of the separated free shear layer, a region of strong pressure fluctuations. The comparison afforded in Fig. 11 suggests that the somewhat similar fluctuations in the transition region of the boundary layer might be responsible for cavitation inception on bodies not having a laminar boundary layer separation.

Surface Nuclei by Electrolysis

We have seen in Fig. 10 that σ_i for the Swedish headform was considerably lower than $-C_{pmin}$ and in some cases even lower than $-C_{p_s}$. The foregoing observation indicates that just prior to incipient conditions, liquid in the neighborhood of the minimum pressure point is under an actual tension. It seemed possible when the present work was started that this tension could not be supported if an abundant supply of surface nuclei were available. Such a supply can be formed by electrolysis and in the present work this was done by making the whole test body the cathode of a d-c circuit. A nonconducting adapter was utilized to isolate the body from the sting assembly and tunnel walls. A voltage pulse of 75 v was applied between the tunnel wall and body to produce electrolysis bubbles. The resulting current density was approximately 0.2 amperes per square in.

The tests to be described were carried out at a constant velocity of 30 fps and at this velocity σ_i under natural conditions was found to be about 0.427; photograph (c) of Fig. 12 illustrates this condition. The first test was carried out for a value of $\sigma = 0.544$ which is less than $-C_{pmin}$ but greater than $-C_{p_s}$ and the normal σ_i; from 12(a), it may be seen that electrolysis bubbles cavitated readily starting from the minimum pressure point. The second test was carried out for a value of $\sigma = 0.437$ which is less than $-C_{pmin}$ and $-C_{p_s}$ but is still greater than σ_i; from 12(b), profuse cavitation from electrolysis bubbles starting slightly earlier than the minimum pressure point is apparent. However, the presence of electrolysis bubbles did not trigger a steady cavity at this pressure and the cavitation observed completely disappeared as soon as the production of electrolysis bubbles was stopped.

From the observations of this type it was determined that with a steady supply of sufficient surface nuclei one can, in fact, observe steady cavitation where $\sigma \doteq -C_{pmin}$. It appears possible therefore that this relationship may be used to determine $-C_{pmin}$ for complex flows. On the Swedish headform, just prior to inception, a considerable portion of the liquid is at pressures below vapor pressure. Even under these conditions a momentary supply of artificial nuclei supplied by electrolysis did not trigger
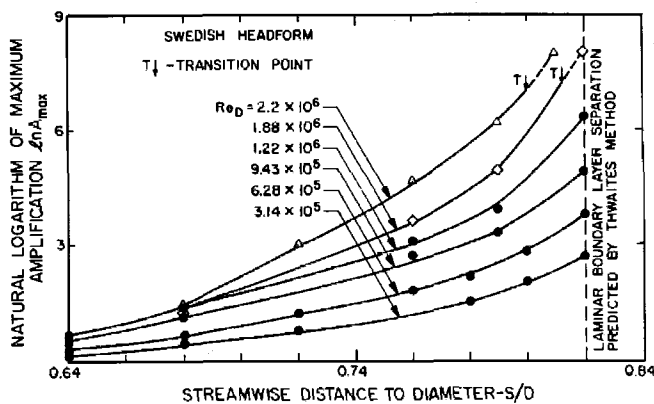
Fig. 13 Calculated maximum amplification factors along streamwise position of the Swedish headform with increasing Reynolds number

a steady attached cavity and such a cavity was not observed until the cavitation number was lowered to its normal inception value.

Acknowledgments

References

1 Knapp, R. T., Daily, J. W., and Hammitt, F. G., *Cavitation*, McGraw-Hill, U.S.A., 1970.

2 Holl, J. W., "Limited Cavitation," *Cavitation State of Knowledge*, ASME, 1969, pp. 26-63.

3 Lindgren, H., and Johnsson, C. A., "Cavitation Inception on Head Forms ITTC Comparative Experiments," Publications of the Swedish State Shipbuilding Experimental Tank, No. 58, 1966. (Also presented at the Eleventh ITTC Meeting, Tokyo, 1966.)

4 Acosta, A. J., and Hamaguchi, H., "Cavitation Inception on the ITTC Standard Head Form," Report No. E.149.1, Hydrodynamics Laboratory, California Institute of Technology, Mar. 1967.

5 Johnson, V. E., and Hsieh, T., "The Influence of the Trajectories of Gas Nuclei on Cavitation Inception," Sixth Symposium on Naval Hydrodynamics, Sept. 1966 (sponsored by ONR).

6 Schiebe, F. R., "The Influence of Gas Nuclei Size Distribution on Transient Cavitation Near Inception," Project Rep. No. 107, St. Anthony Falls Hydraulic Laboratory, University of Minnesota, May 1969.

7 Peterson, F. B., "Hydrodynamic Cavitation and Some Considerations of the Influence of Free-Gas Content," Ninth Symposium on Naval Hydrodynamics, Paris, Aug. 1972.

8 Parkin, B. R., and Kermeen, R. W., "Incipient Cavitation and Boundary Layer Interaction on a Streamlined Body," Report No. E-35.2, Hydrodynamics Laboratory, California Institute of Technology, Dec. 1953.

9 Van der Walle, F., "On the Growth of Nuclei and the Related Scaling Factors in Cavitation Inception," Fourth Symposium on Naval Hydrodynamics, Aug. 27-31, 1962 (sponsored by ONR).

10 Holl, J. W., and Kornhauser, A. L., "Thermodynamic Effects on Desinent Cavitation on Hemispherical Nosed Bodies in Water of Temperatures From 80 Degrees F to 260 Degrees F," *Journal of Basic Engineering*, TRANS. ASME, Series D, Vol. 92, No. 1, Mar. 1970, pp. 44-58.

11 Arndt, R. E. A., and Daily, J. W., "Cavitation in Turbulent Boundary Layers," *Cavitation State of Knowledge*, ASME, 1969, pp. 64-86.

12 Bailey, A. B., "The Relationship Between Flow Separation and Cavitation," Report No. 1111/70, Department of Engineering Science, Oxford University, 1970.

13 Arakeri, V. H., "Viscous Effects in Inception and Development of Cavitation on Axi-Symmetric Bodies," PhD thesis, California Institute of Technology, 1973. (Also available as Report No. E.183.1, Division of Engineering and Applied Science, California Institute of Technology, 1973.)

14 Bland, R. E., and Pelick, T. J., "The Schlieren Method Applied to Flow Visualization in a Water Tunnel," *Journal of Basic Engineering*, TRANS. ASME, Series D, Vol. 84, No. 3, Sept. 1962, pp. 587-592.

15 Hoyt, J. W., "Wall Effect on ITTC Standard Head Shape Pressure Coefficients," Eleventh ITTC Meeting, Tokyo, Apr. 1966.

16 Gaster, M., "The Structure and Behavior of Laminar Separation Bubbles," Revised Aero Report 1181, NPL, England, Mar. 1967. (Also available as British R. and M. Report No. 3595).

17 Jaffe, N. A., Okamura, T. T., and Smith, A. M. O., "Determination of Spatial Amplification Factors and Their Application to Predicting Transition," *AIAA Journal*, Vol. 8, No. 2, Feb. 1970, pp. 301-308.

18 Roshko, A., "Experiments on a Cylinder at High Reynolds Numbers," *Journal of Fluid Mechanics*, Vol. 10, 1961, p. 345.

19 Rouse, H., and McNown, J. S., "Cavitation and Pressure Distribution Head Forms at Zero Angle of Yaw," Studies in Engineering Bulletin 32, State University of Iowa, 1948.

20 Kermeen, R. W., "Some Observations of Cavitation on Hemispherical Head Models," Report No. E-35.1, Hydrodynamics Laboratory, California Institute of Technology, June 1952.

21 Parkin, B. R., and Kermeen, R. W., "The Roles of Convective Air Diffusion and Liquid Tensile Stresses During Cavitation Inception," *Proceedings of IAHR Symposium*, Sendai, Japan, 1962, pp. 17-35.

22 Plesset, M. S., "Bubble Dynamics," *Proceedings of the Symposium on Cavitation in Real Liquids*, ed. by Davies, R., Elsevier Publishing Company, 1964, pp. 1-17.

23 Holl, J. W., and Treaster, A. L., "Cavitation Hysteresis," *Journal of Basic Engineering*, TRANS. ASME, Series D, Vol. 81, No. 1, Mar. 1966, pp. 199-212.

24 Parkin, B. R., and Holl, J. W., "Incipient-Cavitation Scaling Experiments for Hemispherical and 1.5 Calibre Ogive-Nosed Bodies," Report Nord 7958-264, Ordnance Research Laboratory, The Pennsylvania State University, May 1954.

25 Wazzan, A. R., Okamura, T. T., and Smith, A. M. O., "Spatial and Temporal Stability Charts for the Falkner-Skan Boundary Layer Profiles," Report No. DAC67086, McDonnel Douglas Corporation, Sept. 1968.

26 Thwaites, B., "Approximate Calculation of the Laminar Boundary Layer," *Aeronautical Quarterly*, Vol. 1, 1949, pp. 245-280.

27 Crabtree, L. F., Kuchemann, D., and Sowerby, L., "Three Dimensional Boundary Layers," in *Laminar Boundary Layers*, Edited by Rosenhead, L., 1963, pp. 430-432.

APPENDIX

The approximate position of transition was computed with the help of spatial stability charts for the Falkner-Skan boundary layer profiles computed by Wazzan, Okamura, and Smith [25]. Turbulent transition of the boundary layer is said to occur when the amplitude of an initial disturbance is magnified by a factor of exp (7) based on the semiempirical method of Smith [17]. This method was applied for hemispherical nose, Swedish headform, and 1.5 caliber ogive. Necessary local boundary layer quantities such as displacement thickness, shape parameter, etc., were computed by Thwaites' approximate method. The amplification is given as a function of streamwise coordinate along the body surface for the Swedish headform in Fig. 13. It may be noted that for $Re_D < 1.5 \times 10^6$, sufficient amplification in the attached laminar boundary layer prior to predicted position of laminar separation has not taken place and thus for these Reynolds numbers laminar separation will prevail. But, for $Re_D > 1.5 \times 10^6$ sufficient amplification for transition has taken place prior to the point of the predicted laminar separation

and thus presumably there will not be any laminar separation. Therefore for the Swedish headform $Re_{D_{crit}} \doteq 1.5 \times 10^6$. Similar diagrams [13] showed that $Re_{D_{crit}} \doteq 5 \times 10^6$ for the hemispherical nose and $Re_{D_{crit}} \doteq 6.3 \times 10^5$ for the 1.5 caliber ogive. Computed streamwise positions of the location of transition point for Re_D greater than 6.3×10^5 for 1.5 caliber ogive are tabulated in the following:

Reynolds number—Re_D	Computed position of transition—$(S/D)_{tr}$
9.43×10^5	1.296
1.25×10^6	1.28
1.57×10^6	1.254
1.88×10^6	1.21
2.2×10^6	1.202